Analysis of gene expression changes in the spinal cord during chronic pain and function of CDKL5 as a neurite outgrowth-promoting protein

(慢性疼痛モデルマウスの脊髄における遺伝子発現変化と神経突起伸長促進タンパク質としての CDKL5 の機能に関する検討)

千葉大学大学院医学薬学府

先端医学薬学専攻

主任：大鳥精司教授

穂積　崇史

Abstract

Background: Chronic pain is a highly refractory and complicated condition that persists even without nociception. Several genome-wide analysis of gene expression reported the immune response and inflammatory cytokine affect chronic pain establishment since the early phase of pain. However, compared to the acute phase, the chronic phase's gene expression profile is poorly analyzed.

Methods: We established the mouse sciatic nerve cuff model as a neuropathic pain model by placing a 2mm section of split PE-20 polyethylene tube around the sciatic nerve. The spinal cord at L4-6 level was harvested 28 days after surgery. We then examined differentially expressed genes (DEGs) by RNA sequence (RNA-seq) compared with the sham group and conducted enrichment analyses of expressed genes. To reveal the characteristics of chronic pain, we compared the gene expression profiles of spinal cord between the acute and chronic phases in the neuropathic pain model. Among the genes categorized in the dendrite in chronic pain, we focused on cyclin-dependent kinase-like 5 (CDKL5). We analyzed the expression and function of CDKL5 with real-time polymerase chain reaction (PCR), immunohistochemistry, and neurite extension assay in Neuro 2a (N2a) cells. Three types of CDKL5 plasmid were used, encoding wild type, nuclear localization signal (NLS)-attached, and K42R kinase-dead CDKL5.

Results: We defined 403 DEGs, including 104 upregulated genes and 43 downregulated genes (FDR<0.01). Instead of inflammation or immune response, the most enriched terms in the chronic phase were "regulation of plasma membrane-bounded cell projection organization" and "dendrite." We focused on CDKL5 from genes categorized to the "dendrite" term. Real-time PCR assay validated the increased expression of *CDKL5* in the ipsilateral dorsal horn. CDKL5 was expressed broadly in the ipsilateral dorsal horn across layers. Neurite extension assay showed the cytoplasmic kinase function of CDKL5 was required for neurite outgrowth in N2a cells.

Conclusion: RNA-seq of spinal cord revealed the most enriched genes in chronic phase were related to the regulation of axon and dendrite morphogenesis, including CDKL5. Our results indicated that neural remodeling could affect the establishment of chronic pain. Since patients with CDKL5 mutation reportedly show a deficiency in pain perception in humans, our findings raise the possibility CDKL5 in the spinal cord could cause the neural remodeling of chronic pain phase thorough cytoplasmic kinase activity.

Keywords:

Neuropathic pain, Chronic Pain, Spinal Cord, RNA-seq, neurite outgrowth, CDKL5

Abbreviations:

ARHGEF2, Rho guanine nucleotide exchange factor 2; BDNF, brain-derived neurotrophic factor; BSA, bovine serum albumin; CCI, chronic constriction injury; CCL2, C-C motif chemokine; CDKL5, cyclin-dependent kinase-like 5; CGRP, calcitonin gene-related peptide; con, contralateral; DAPI, 4’,6-diamidino-2-phenylindole; DEG, differentially expressed gene; DMEM, Dulbecco's modified Eagle's medium; EB2, EB family member 2; FABP1, fatty acid binding protein 1; FBS, fetal bovine serum; FDR, false discovery rate; FPKM, fragments per kilobase of exon per million reads mapped; GEO, gene expression omnibus; GFP,

green fluorescent protein; GO, gene ontology;GRIN2A, glutamate ionotropic receptor NMDA type subunit 2A; HEK293, human embryonic kidney cells 293; Iba1, Ionized calcium binding adapter protein; IL1β, interleukin 1 beta; ips, ipsilateral; K42R, Lys42Arg; KEGG, Kyoto encyclopedia of genes and genomes; mRNA, messenger RNA; MAP1S, microtubule-associated protein 1S; N2a, neuro-2a; NeuN, neuronal nuclei; NLS, nuclear localization signal; PBS, phosphate buffered saline; PCR, polymerase chain reaction; PFA, paraformaldehyde; PNI, peripheral nerve injury; Rac1, RAS-related C3 botulinus toxin substrate 1; RIN, RNA integrity numbers; RNA-seq, RNA sequence; SEM, standard error of the mean; SNI, spared nerve injury; TNFα,tumor necrosis factor alpha; VGLUT1, vesicular glutamate transporter 1; WT, wild type;

Funding: This research did not receive any specific grant from funding agencies in the public, commercial, or not-for-profit sectors.

Introduction

Unlike acute pain as a signal of damage or danger, chronic pain is a highly refractory and complicated condition that persists even without nociception. There is no effective treatment, and chronic pain affects more than 200,000 people worldwide [1]. Especially, Neuropathic pain caused by damage or dysfunction of the nerve system often becomes chronic. Several neuropathic pain models have been established and used to analyze the mechanism of chronic pain [2]. According to previous reports, the functional changes in pain pathways caused by an immune response and inflammatory cytokine release in the pain pathways affect chronic pain. In the spinal cord, peripheral nerve injury activates microglia, and it releases inflammatory cytokines such as TNFα, IL1β, and BDNF, which change the excitability of excitatory/inhibitory interneurons [3,4]. Astrocytes are also activated later for microglia and maintain persistent pain [5]. In addition to these functional changes, anatomical changes such as spine remodeling and synapse reorganization are involved in chronic pain [6]. However, the molecular mechanism of chronic pain is still unclear. Thus, to improve understanding of pathogenesis in neuropathic pain is essential to develop therapeutic strategies.

Several reports assessed gene expression profiles to evaluate the molecular mechanism underlying chronic pain development and sustention. In previous studies, the genes and pathways related to inflammation and immune response were upregulated in the spinal cord of neuropathic pain model using microarrays and RNA-seq [7,8,9]. These studies were mostly based on the data of acute pain phase, however the mechanisms other than inflammation might be involved in the development and maintenance of chronic pain, which could be prominent therapeutic targets for chronic pain.

In the present study, we profiled gene expression in the spinal cord of neuropathic pain mouse model at chronic phase. We then compared our results with previously reported RNA-seq data in the acute phase [9] to reveal features of chronic pain. Furthermore, we focused on a specific gene, *CDKL5*, and examined its expression in the spinal cord and the neural function *in vitro*.

Material and methods

Sciatic Nerve Cuff Model

Male 6-8 weeks old C57/BL6J mice were purchased from Japan SLC Inc. (Shizuoka, Japan) and allowed to acclimate for a minimum of 7 days before the experimental procedure. We housed all mice under a 12 h light/dark cycle at room temperature.

We used the sciatic nerve cuff model previously described [10,11]. Briefly, we anesthetized mice by intraperitoneal injection with a combination of anesthetic (0.3 mg/kg of medetomidine, 4.0 mg/kg of midazolam, and 5.0 mg/kg of butorphanol). Then we made a small incision at the right midthigh and bluntly exposed the right sciatic nerve's common branch. A 2 mm section of split PE-20 polyethylene tube (inner diameter: 0.35 mm, outer diameter: 1.05 mm, Natsume Seisakusho Co., Tokyo) was placed around it. We closed the cuff gently with the pliers applying pressure on both sides of the tube without squeezing and turned the make sure the proper closure. The cuffed nerve was replaced to its normal position, and the fascia and the skin were closed with 4-0 nylon sutures. Sham-operated mice underwent the same surgical procedure

without cuff implantation. There were four groups: postoperative seven days (d7), 14 days (d14), 28 days (d28) after sciatic nerve cuffing surgery groups (cuff group), and sham surgery group (sham group) as control. We made all efforts to minimize animal suffering and the number of animals used. All animal experiments were approved by the Institutional Animal Care and Use Committee at Chiba University.

Nociceptive testing

The right hind paw's mechanical hypersensitivity was measured by assessing 50% withdrawal thresholds using von Frey filaments (0.02-4g, MUROMACHI KIKAI, Tokyo, Japan), following an up-down method as previously described [12]. Mice were randomized and acclimated to the test chamber for one hour before performing behavioral tests. We placed mice in individual plexiglass cage with a wire mesh bottom, allowing full access to the paws. We applied the von Frey filament to the plantar surface of the paw. The stimulus strength was gradually increased or decreased to determine the withdrawal threshold. We obtained baseline thresholds a day before surgery. Tests were performed every week for one month after surgery.

Immunohistochemistry

Mice were perfused intracardially with 4% PFA. Spinal Cord at L4-6 lumbar level was harvested and post-fixed in 4% PFA overnight at 4 ℃. Samples were then transferred into 30% sucrose overnight for cryoprotection and then rapidly frozen. Spinal cord sections cut in 30μm-thick with a cryostat were permeabilized in PBS containing 0.3% Triton-X 100 with 5% BSA, and then, blocked in blocking solution [PBS containing 0.1% Triton X-100, 5% BSA]. Samples were incubated overnight at 4 ℃ with a primary antibody diluted in a blocking solution. The primary antibodies used were anti-Iba1 (1:100, WAKO, #019–19,741), anti CDKL5 (1:100, Sigma-Aldrich, #HPA002847), anti-CGRP (1:00, Santa Cruz, #sc-57053), anti-VGLUT1 (1:100, Santa Cruz, #sc-377425), anti-NeuN (1:100, Sigma-Aldrich, #MAB377), and anti-FLAG (1:100, Sigma-Aldrich, #F3165).

After washed three times in PBS, sections were incubated with secondary antibody (1:1000, Invitrogen, A11004, 11008, 11011) at room temperature for 1 hour. We obtained images using the FSX100 microscope system (Olympus, Tokyo, Japan) and analyzed obtained Images with Image J software (http://rsbweb.nih.gov/ij/download. HTML). We compared four independent areas for their intensities of the antibody-positive area/analyzed area. Data were shown as fold change vs. control ± SEM, and p values were determined with Dunnett's test (*$p<0.05$ was considered significant) with Statcel software (OMS Publishing Inc., Tokyo, Japan).

RNA isolation

Total RNAs were extracted from the spinal cord at L4-6 level with RNAiso Plus (Takara Bio., Japan) and purified with the NucleoSpin RNA purification kit (Takara Bio., Japan) with on-column DNase I digestion. The RIN was evaluated using Agilent 2100 Bioanalyzer (Agilent Technologies, Palo Alto, CA). This indicator was > 8 in all the samples.

Real-time PCR assay

Total RNAs were extracted from the spinal cords at the L4-6 level of cuff group mice at day 7, 14, 28, and sham-operated group mice using RNAIso-PLUS (Takara Bio, Japan). RNA (0.5 μg) was reverse transcribed to produce cDNA using ReverTra Ace® qPCR RT Kit with gDNA remover (TOYOBO, Japan). Real-time PCR was performed using THUNDERBIRD® SYBR® qPCR Mix (TOYOBO, Japan). We performed all real-time PCR assays in biological triplicate using the 7300 Real-Time PCR System (Applied Biosystems). We used 18s ribosomal primers to standardize relative mRNA expression. The forward(F) and reverse(R) primers were: m18s F, 5' -GCAATTATTCCCCATGAACG; m18s R, 5'-GGCCTCACTAAACCATCCAA; mCCL2 F, 5'-CTCCAGCCTACTCATTGGGATCA; mCCL2 R, 5'-GCATCCACGTGTTGGCTCA; mCDKL5 F, 5'-TTGGGGTTGTCGGTGAAGG; mCDKL5 R, 5'-TTAAGCTCTCGTAAGGTCGTCT. The cycle threshold values (Ct values) were calculated by the ΔΔCt method to obtain the fold changes. Four spinal cords were used for real-time PCR analysis at each time point. We expressed data as fold changes vs. sham group ± SEM. The asterisks indicate a statistically significant difference ($*p < 0.05$), Dunnett's multiple comparison test with Statcel software (OMS Publishing Inc., Tokyo, Japan).

RNA-sequencing library construction, sequencing, and analyses

We harvested the mice's spinal cord's total RNAs in the d28 and the sham group (4 mice/group). Two samples out of four samples were pooled together, and two samples for each group were made. And then, we sent these samples to the Macrogen Japan Corp. (Kyoto, Japan). Transcriptomes of 4 samples were analyzed by RNA-seq, as described previously [13]. Briefly, 1 μg of the total RNA was analyzed using the TruSeq RNA library kit to construct the cDNA libraries. The protocol included polyA-selected RNA extraction, RNA fragmentation, random hexamer primed reverse transcription, and 100 nt paired-end sequencing using an Illumina NovaSeq6000 (Illumina, San Diego, CA, USA). According to the Quantification Protocol Guide, the libraries were quantified using real-time PCR.

Data availability

We deposited raw RNA-seq data in NCBI's GEO. They are accessible through GEO Series accession number GSE162574.

Data analysis

Quality Control: To remove technical sequences, including adapters, PCR primers, or fragments thereof, and quality of bases lower than 20, pass filter data of FASTQ format were processed Trimmomatic (v0.30) to be high-quality clean data.

Mapping: Firstly, we downloaded reference genome sequences and gene model annotation files of related species from the genome website (UCSC, NCBI, ENSEMBL). Secondly, Hisat2 (v2.0.1) was used to index the reference genome sequence (mm10). Finally, we aligned clean data to the reference genome via software Hisat2 (v2.0.1).

Expression analysis: In the beginning, transcripts in FASTA format are converted from known gff annotation

files and indexed properly. Then, with the file as a reference gene file, FeatureCounts estimated gene and isoform expression levels from the pair-end clean data.

Differential expression analysis: To analyze differential expressed genes, we used the Dseq2 method with online software TCC-GUI (https://infinityloop.shinyapps.io/TCC-GUI/) [14] and iDEP (http://ge-lab.org/idep/) [15]. FDR was set < 0.01 to detect differential expressed ones.

Bioinformatics analysis: The GO terms, including and KEGG pathway enrichment analysis, were performed for DEGs using David (https://david.ncifcrf.gov/) [16] and Metascape (http://metascape.org/) [17], a gene annotation, and analysis resource.

Hierarchical clustering analysis: Hierarchical clustering analysis is to group samples or genes with similar expression patterns by calculating and classifying the data according to similarities. This clustering helps predict unknown genes' function and whether they are involved in the same metabolic process or cellular pathway. Genes with similar expression patterns are within the same cluster and close to each other, and they may have similar functions or participate in the same biological processes.

RNA-seq data of acute-phase mouse pain model

We obtained the reported RNA-seq data that analyzed the spinal cord's genetic profile of the neuropathic pain model one week after surgery (available at http://links.lww.com/PAIN/A714) [9]. We compared this as an acute phase profile with the current result as a chronic phase profile. We selected DEGs satisfying $p<0.05$ and analyzed them using Metascape (http://metascape.org/) to compare the enriched terms.

DNA construct, cell culture, and transfection

We obtained three types of plasmid DNA constructs of CDKL5 (WT, NLS-attached, and K42R kinase-dead mutant) from MRC PPU (http://mrcppureagents.dundee.ac.uk/reagents-view-cdna-clones/616152) [18]. WT and K42R kinase-dead CDKL5 were fused with GFP, and NLS-attached CDKL5 was tagged with FLAG. We transfected each plasmid DNA into HEK293 cells and assessed the subcellular localization of CDKL5 in the cells with micro-fluoroscopy 24hour after transfection. HEK293 cells were cultured in DMEM supplemented with 10% FBS in a 5% CO2 atmosphere at 37℃. Transient transfections were performed using Lipofectamine 2000 (Invitrogen) according to the manufacturer's instructions.

Neurite extension assay

We cultured N2a cells in DMEM supplemented with 10% FBS in a 5% CO2 atmosphere at 37℃. We transfected each plasmid DNA into N2a cells as described above.

We transfected each three types of plasmid DNA with an empty plasmid encoding GFP by the ratio of 5:1 into N2a cells. These cells were cultured for 24h in DMEM containing 10% fetal bovine serum and then were plated onto 30mm-dishes and differentiated in differentiating cell media [DMEM + 2% FBS] for 36h at the concentration of 3-5×106 /mm [19].

The neuron with neurite longer than the diameter of the cell body was determined “neurite-bearing” cell. We calculated the percentage of the "neurite-bearing" cells evaluating four different fields of each dish using the FSX100 microscope system (Olympus, Tokyo, Japan).

Results

Model-identification of neuropathic pain

The neuropathic pain was established by cuffing to the right sciatic nerve in mice (Fig.1A). Mechanical hypersensitivity developed rapidly following sciatic nerve cuffing and persisted for at least 28 days only on the hind paw (Fig.1B). CCL2 is a chemokine associated with inflammation, and CCL2 is upregulated transcriptionally the neuropathic pain model [20,21]. In the current study as well, CCL2 was upregulated and peaked at d7 in the spinal cord by real-time PCR assay (Fig.1C).

To examine the activation of microglia, we performed immunostaining with anti-Iba1 (a marker of microglia) antibody. Iba1 staining revealed microglial proliferation in the dorsal horn ipsilateral to cuff surgery. Iba1 expression peaked at d7 and decreased at d28 (Fig.1D).

Differential expressed genes and TOP up/down-regulated genes in the spinal cord.

To investigate the underlying mechanism of chronic pain, we analyzed the gene expression profile of L4-6 level spinal cord at d28, by RNA-seq.

We identified 403 DEGs between the cuff and sham group in FDR<0.01 (Fig. 2A). The heat map visualized the expression levels for each gene. The hierarchical clustering classified the d28 and sham groups into separated categories (Fig.2B). We defined the up/down-regulated genes when their change was larger than 2-fold. These 403 genes included 104 upregulated genes and 43 downregulated genes. Mostly upregulated genes were *Sacsin*, that is thought to function in chaperon-mediated protein folding, and *GRIN2A*, that encodes NMDA receptor subunit. The most downregulated gene was *FABP1* known as a liver-type fatty acid-binding protein. Each top 20 genes are shown in Fig. 2C, D.

Enrichment analysis and comparison between the acute and chronic phase of pain

We compared the gene expression profiles between the acute and chronic phases in the neuropathic pain model to reveal the characteristics of chronic pain. We used the available RNA-seq result of the spinal cord in neuropathic pain model 7d after surgery as an acute phase data [9].

A large number of the DEGs were categorized as inflammation and immune response in the acute phase (Fig.3A). On the other hand, the most categorized terms of our results using chronic phase samples were “regulation of plasma membrane-bounded cell projection organization” and “dendrite” (Fig.3B). Based on the biological process in the GO term, the term "Regulation of plasma membrane-bounded cell projection” was defined as the process that modulates the process involved in the formation, arrangement of constituent parts, or disassembly of plasma membrane-bounded cell projections, which include a cilium or axon. The term “dendrite” was defined as the process whose specific outcome is the dendrite's progression over time, from its formation to the mature structure. Thus, the terms related to structural change or remodeling of neurons were upregulated in the chronic phase.

The heatmap provides a visual representation of the differentiation of mostly categorized terms between two groups. Many terms, mostly enriched in the acute phase, were not upregulated in the chronic phase (Fig.3C). The circos map also represented the difference between the two groups. Only a small number of terms were

categorized concurrently in both groups (Fig.3D).

Real-time PCR validation for *CDKL5* gene expression

Among the genes classified as "dendrite," we focused on CDKL5 because its mutation can cause a deficiency in pain perception in humans [22]. We harvested the ipsilateral dorsal horn of sham and cuff model mice d7 after surgery and validated the expression of CDKL5 mRNA using real-time PCR. CDKL5 mRNA expression was significantly higher in the cuff group than in the sham group (Fig. 4A).

CDKL5 expression in the spinal cord of neuropathic pain model

To examine the expression pattern of CDKL5 in the spinal cord, we performed an immunohistochemistry assay. Our immunohistochemical analysis showed the CDKL5-positive cells were widely distributed. CGRP is a marker of peptidergic C fibers that mainly projects to lamina I and lamina IIo, while VGLUT1 is a marker of myelinated A fiber that mainly projects to lamina III. Co-staining with CGRP and VGLUT1 did not detect a distinct expression difference of CDKL5 between layers (Fig. 4B1-4B4). CDKL5-expressing cells were positive with NeuN, a marker of a neuron (Fig. 4B5-4B7). Higher magnification images showed that CDKL5 was mostly expressed in the cytoplasm with a punctuated pattern. (Fig. 4B8-4B9).

The kinase activity of CDKL5 in the cytoplasm is required to extend neurite

Ectopic CDKL5 expression induced the neurite extension in previous studies [23]. However, the underlying mechanism is still unclear. CDKL5 is a cyclin-dependent kinase intracellularly present in both the nucleus and cytoplasm in brain neurons [24]. To know whether kinase activity or subcellular localization is critical for the effect of neurite extension, we used two CDKL5 mutant DNA constructs, encoding K42R kinase-dead and NLS-attached CDKL5.

First, we examined the subcellular localization of two CDKL5 mutants in HEK293 cells. WT and K42R kinase-dead CDKL5 were distributed in both the nucleus and cytoplasm, while NLS-attached CDKL5 was only distributed in the nucleus of HEK293 cells. (Fig. 5A, B). Then to assess the functional change due to subcellular localization and kinase activity, we transfected three types of CDKL5 plasmid into N2a cells and examined neurite outgrowth, respectively. The percentage of "neurite-bearing" cells was significantly higher in the WT CDKL5 group than that of the control group. There was no increase in the NLS-attached and K42R kinase-dead group compared to the control (Fig. 5C, D).

Discussion

To evaluate the gene expression profile in the spinal cord of the chronic pain mice, we performed RNA-seq four weeks after cuff surgery. A total of 403 DEGs were found, including 104 upregulated and 36 downregulated genes (FDR<0.01). GO and KEGG biological pathway analysis showed that most genes belonged to the term of formation and regulation of process extending from a cell, e.g., a cilium, axon, or dendrite. This profile differed from the reported one of the acute phase, in which the term of inflammation and immune response were mostly enriched.

The neuropathic pain model used in this study, the cuff model, is widely used as a neuropathic pain model, like CCI [25] or SNI [26]. This model causes mechanical allodynia by introducing a correctly sized cuff to a sciatic nerve, and the allodynia lasts 60 days [27]. Our model represented persistent allodynia, which is consistent with previous reports. In general, the glial cells are activated in the peripheral neuropathy condition. Microglia get increased, and hypertrophic is the affected side of the spinal dorsal horn, and that reaction peaked at seven days after PNI surgery [28]. Following microglial activation, astrocytes also get activated and release cytokines. CCL2 is a chemokine associated with inflammation and enhances microglia and excitatory neurons [20]. CCL2 is expressed in the astrocytes in the pain condition, and its expression peaked at three days after SNL surgery [29]. Microglial activation and CCL2 expression in the current study were consistent with these studies, indicating the pain model was well established.

Previous genome-wide analysis of gene expression has reported the upregulation of genes related to inflammation and immune response in the spinal cord of the neuropathic pain model [9]. Neural inflammation affects pain transmission pathways and causes hypersensitivity, and the relationship between pain and inflammation has been studied broadly. However, these studies analyzed gene profiles in the acute period of 1-2 weeks after the pain model creation, and few reports analyzed them on the chronic phase. In the current study, the chronic pain phase's gene expression profile was different from that of the acute phase, as heatmap and circos map showed. In chronic phase, many upregulated genes belonged to the term regulating the neural axon and dendrite formation instead of inflammation or immune response. Structural remodeling of the neuron has been discussed recently as one of the possible mechanisms of chronic pain. Persistent pain stimuli cause density enhancement and structural change of the spine [30]. The relationship between structural changes and pain is still controversial, but it may be one of the mechanisms making chronic pain.

Among the genes categorized in the dendrite, we focused on CDKL5. CDKL5 is an X-linked kinase protein gene, and its mutations is known as the cause of infantile epilepsy syndrome characterized by early-onset epileptic encephalopathy and severe intellectual disability [22,31]. Furthermore, a substantial percentage of CDKL5 deficiency has an anamnestic deficiency in pain perception, and the relationship between CDKL5 and pain has attracted attention these days [32]. CDKL5 is expressed mainly in the brain's nerve cells and is intracellularly present in both the nucleus and cytoplasm [24], especially in excitatory synapses [34,35]. By local protein synthesis, CDKL5 affects remodeling and stabilization of the spine and synapse in adult neurons [24]. A recent report showed that CDKL5 is highly expressed in gliomas, and CDKL5 overexpression promotes invasion, proliferation, and migration [31]. In our study, CDKL5 overexpression also promoted neurite outgrowth. Besides, NLS-attached and K42R kinase-dead mutants did not promote process elongation. It indicates that exerting kinase activity in the cytoplasmic region instead of the nucleus leads to neurite outgrowth. The mechanism of CDKL5's control over dendrite morphogenesis is not completely understood. Based on the previous studies, this function is mediated by the interaction of CDKL5 and Rac1 [23,35]. Microtubule-associated proteins EB2, MAP1S, and ARHGEF2, were reported to be CDKL5 substrates in microtubule dynamics [36]. Besides, kinase activity seems essential for this function [23], which would be consistent with our results.

In general, CDKL5 is expressed in excitatory neurons in the brain. CDKL5 was seemingly expressed widely in excitatory interneurons of the dorsal horn. Immunostaining was performed on spinal dorsal horn samples to examine protein expression. However, we observed no significant difference between the bilateral dorsal horn. Since CDKL5 expression change was presumed to occur locally in the remodeling sites such as the spine, the microstructural changes could not be visualized by immunostaining of spinal cord sections in our study using commercially available antibodies.

There are several limitations to this study. First, we did not assess the gene expression profiles in the acute phase by ourselves. Besides, a longer follow-up and analysis in the more chronic phase are also needed in further study. Second, our immunohistochemical analysis could not detect the distribution feature of CDKL5 in the spinal cord. We had tried four types of commercially available anti-CDKL5 antibodies, but only one antibody was useful for immunostaining. However, we were unable to detect the detailed distributions of CDKL5 in dendrites or axons in the spinal cord by this antibody. Further study is needed using antibodies of better performances. Finally, the analysis for CDKL5 substrates working in neural remodeling (e.g., microtubule dynamics) is also needed in the future.

Conclusion

We analyzed the gene expression profile of the spinal cord in the chronic pain model mouse. Most enriched terms in the chronic phase were related to the regulation of axon and dendrite morphogenesis. Our results indicated that neural remodeling could affect the establishment of chronic pain. Furthermore, CDKL5 present in the cytoplasm could cause neural remodeling of chronic pain.

Reference

[1] de Souza, J.B., Grossmann, E., Perissinotti, D.M.N., 2017. Prevalence of Chronic Pain, Treatments, Perception, and Interference on Life Activities: Brazilian Population-Based Survey. Pain Res Manag. 4643830. https://doi.org/10.1155/2017/4643830.

[2] Jaggi, A.S., Jain, V., Singh, N., 2011. Animal models of neuropathic pain. Fundam Clin Pharmacol. 25(1), 1-28. https://doi.org/10.1111/j.1472-8206.2009.00801.x.

[3] Austin, P.J., Moalem-Taylor, G., 2010. The neuro-immune balance in neuropathic pain: involvement of inflammatory immune cells, immune-like glial cells and cytokines. J Neuroimmunol. 229(1-2), 26-50. https://doi.org/10.1016/j.jneuroim.2010.08.013.

[4] Tsuda, M., 2019. Microglia-Mediated Regulation of Neuropathic Pain: Molecular and Cellular Mechanisms. Biol. Pharm. Bull. 42(12), 1959-1968. https://doi.org/10.1248/bpb.b19-00715.

[5] Tsuda, M., Kohro, Y., Yano, T., 2011. JAK-STAT3 pathway regulates spinal astrocyte proliferation and neuropathic pain maintenance in rats. Brain. 134(4), 1127-1139. https://doi.org/10.1093/brain/awr025.

[6] Kuner, R., Flor, H., 2016. Structural plasticity and reorganisation in chronic pain. Nat Rev Neurosci. 18(1), 20-30. https://doi.org/10.1038/nrn.2016.162.

[7] Du, H., Shi, J., Wang, M., 2018. Analyses of gene expression profiles in the rat dorsal horn of the spinal cord using RNA sequencing in chronic constriction injury rats. J Neuroinflammation. 15(1), 280. https://doi.org/10.1186/s12974-018-1316-0.

[8] Costigan, M., Moss, A., Latremoliere, A., 2009. T-cell infiltration and signaling in the adult dorsal spinal cord is a major contributor to neuropathic pain-like hypersensitivity. J Neurosci. 29(46), 14415-14422. https://doi.org/10.1523/JNEUROSCI.4569-09.2009.

[9] Parisien, M., Samoshkin, A., Shannon N.T., 2019. Genetic pathway analysis reveals a major role for extracellular matrix organization in inflammatory and neuropathic pain. Pain. 160(4), 932-944. http://dx.doi.org/10.1097/j.pain.0000000000001471.

[10] Mosconi, T., Kruger, L., 1996. Fixed-diameter polyethylene cuffs applied to the rat sciatic nerve induce a painful neuropathy: ultrastructural morphometric analysis of axonal alterations. Pain. 64(1), 37-57. https://doi.org/10.1016/0304-3959(95)00077-1.

[11] Benbouzid, M., Pallage, V., Rajalu, M., 2008. Sciatic nerve cuffing in mice: a model of sustained neuropathic pain. Eur J Pain. 12(5), 591-599. https://doi.org/10.1016/j.ejpain.2007.10.002.

[12] Chaplan, S.R., Bach, F.W., Pogrel, J.W., 1994. Quantitative assessment of tactile allodynia in the rat paw. J Neurosci Methods. 53(1), 55-63. https://doi.org/10.1016/0165-0270(94)90144-9.

[13] Kim, J.E., Hong, Y.H., Kim, J.Y., 2017. Altered nucleocytoplasmic proteome and transcriptome distributions in an in vitro model of amyotrophic lateral sclerosis. PLoS One. 12(4), e0176462. https://doi.org/10.1371/journal.pone.0176462.

[14] Su, W., Sun, J., Shimizu, K., 2019. TCC-GUI: a Shiny-based application for differential expression analysis of RNA-Seq count data. BMC Res Notes. 12(1), 133. https://doi.org/10.1186/s13104-019-4179-2.

[15] Ge, S.X., Son, E.W., Yao, R., 2018. iDEP: an integrated web application for differential expression and pathway analysis of RNA-Seq data. BMC Bioinformatics. 19(1), 534. https://doi.org/10.1186/s12859-018-

2486-6.
[16] Huang, Q., Zheng, Y., Ou, Y., 2019. Retraction notice to “miR-34a/Bcl-2 signaling pathway contributes to agerelated hearing loss by modulating hair cell apoptosis” [Neurosci. Lett. 661 (November) (2017) 51–56]. Neurosci Lett. 707, 134290. https://doi.org/10.1016/j.neulet.2019.134290.
[17] Zhou, Y., Zhou, B., Pache, L., 2019. Metascape provides a biologist-oriented resource for the analysis of systems-level datasets. Nat Commun. 10(1), 1523. https://doi.org/10.1038/s41467-019-09234-6.
[18] Munoz, I.M., Morgan, M. E., Peltier, J., 2018. Phosphoproteomic screening identifies physiological substrates of the CDKL5 kinase. EMBO J. 37(24), e99559. https://doi.org/10.15252/embj.201899559.
[19] Shi, Q., Li, C., Li, K., 2017. Pallidin protein in neurodevelopment and its relation to the pathogenesis of schizophrenia. Mol Med Rep. 15(2), 665-672. https://doi.org/10.3892/mmr.2016.6064.
[20] Zhang, Z.J., Jiang, B.C., Gao, Y.J., 2017. Chemokines in neuron-glial cell interaction and pathogenesis of neuropathic pain. Cell Mol Life Sci. 74(18), 3275-3291. https://doi.org/10.1007/s00018-017-2513-1.
[21] Al-Mazidi, S., Alotaibi, M., Nedjadi, T., 2018. Blocking of cytokines signalling attenuates evoked and spontaneous neuropathic pain behaviours in the paclitaxel rat model of chemotherapy-induced neuropathy. Eur J Pain. 22(4), 810-821. https://doi.org/10.1002/ejp.1169.
[22] La Montanara, P., Rusconi, L., Locarno, A., 2015. Synaptic synthesis, dephosphorylation, and degradation: a novel paradigm for an activity-dependent neuronal control of CDKL5. J Biol Chem. 290(7), 4512-4527. https://doi.org/10.1074/jbc.M114.589762.
[23] Chen, Q., Zhu, Y.C., Yu, J., 2010. CDKL5, a protein associated with rett syndrome, regulates neuronal morphogenesis via Rac1 signaling. J Neurosci. 30(38), 12777-12786. https://doi.org/10.1523/JNEUROSCI.1102-10.2010.
[24] Zhu, Y.C., Xiong, Z.Q., 2019. Molecular and Synaptic Bases of CDKL5 Disorder. Dev Neurobiol. 79(1), 8-19. https://doi.org/10.1002/dneu.22639.
[25] Bennett, G.J., Xie, Y.K., 1988. A peripheral mononeuropathy in rat that produces disorders of pain sensation like those seen in man. Pain. 33(1), 87-107. https://doi.org/10.1016/0304-3959(88)90209-6.
[26] Decosterd, I., Woolf, C.J., 2000. Spared nerve injury: an animal model of persistent peripheral neuropathic pain. Pain. 87(2), 149-158. https://doi.org/10.1016/S0304-3959(00)00276-1.
[27] Yalcin, I., Bohren, Y., Waltisperger, E., 2011. A time-dependent history of mood disorders in a murine model of neuropathic pain. Biol Psychiatry. 70(10), 946-953. https://doi.org/10.1016/j.biopsych.2011.07.017.
[28] Kohno, K., Kitano, J., Kohro, Y., 2018. Temporal Kinetics of Microgliosis in the Spinal Dorsal Horn after Peripheral Nerve Injury in Rodents. Biol Pharm Bull. 41, 1096-1102. https://doi.org/10.1248/bpb.b18-00278.
[29] Gao, Y.J., Zhang, L., Samad, O.A., 2009. JNK-induced MCP-1 production in spinal cord astrocytes contributes to central sensitization and neuropathic pain. J Neurosci. 29(13), 4096-4108. https://doi.org/10.1523/JNEUROSCI.3623-08.2009.
[30] Tan, A.M., Samad, O.A., Fischer, T.Z., 2012. Maladaptive dendritic spine remodeling contributes to diabetic neuropathic pain. J Neurosci. 32(20), 6795-6807. https://doi.org/10.1523/JNEUROSCI.1017-12.2012.

[31] Jiang, Z., Gong, T., Wei, H., 2019. CDKL5 promotes proliferation, migration, and chemotherapeutic drug resistance of glioma cells via activation of the PI3K/AKT signaling pathway. FEBS Open Bio. 10(2), 268-277. https://doi.org/10.1002/2211-5463.12780.

[32] La Montanara, P., Hervera, A., Baltussen, L.L., 2020. Cyclin-dependent–like kinase 5 is required for pain signaling in human sensory neurons and mouse models. Sci Transl Med. 12(551), eaax4846. https://doi.org/10.1126/scitranslmed.aax4846.

[33] Ricciardi, S., Ungaro, F., Hambrock, M., 2012. CDKL5 ensures excitatory synapse stability by reinforcing NGL-1-PSD95 interaction in the postsynaptic compartment and is impaired in patient iPSC-derived neurons. Nat Cell Biol. 14(9), 911-23. https://doi.org/10.1038/ncb2566.

[34] Zhu, Y.C., Li, D., Wang, L., 2013. Palmitoylation-dependent CDKL5-PSD-95 interaction regulates synaptic targeting of CDKL5 and dendritic spine development. Proc Natl Acad Sci USA. 110(22), 9118-9123. https://doi.org/10.1073/pnas.1300003110.

[35] Luo, L., 2002. Actin cytoskeleton regulation in neuronal morphogenesis and structural plasticity. Annu Rev Cell Dev Biol. 18, 601-635. https://doi.org/10.1146/annurev.cellbio.18.031802.150501.

[36] Baltussen, L.L., Negraes, P.D., Silvestre, M., 2018. Chemical genetic identification of CDKL5 substrates reveals its role in neuronal microtubule dynamics. EMBO J. 37(24), e99763. https://doi.org/10.15252/embj.201899763.

Figure legends

Figure 1. Establishment of a neuropathic pain model.

We implanted the PE-20 polyethylene tube into the right sciatic nerve.

A. Schematic illustration of the sciatic nerve cuffing.

We implanted the PE-20 polyethylene tube into the right sciatic nerve.

B. Nociceptive behavior development in the cuff and sham group mice.

Mechanical withdrawal threshold significantly decreased in the ipsilateral hind paw of cuff group mice. $^{**}p < 0.01$. Dunnett's test (compared to the sham group). N=4 for each time point (sham, d7, d14, d28). Data are expressed as mean ± SEM.

C. CCL2 gene regulation in the spinal cord following sciatic nerve cuffing.

We performed real-time PCR assay at d7, d14, and d28 after sciatic nerve cuffing compared to the sham group. $^{**}p < 0.01$. Dunnett's test (compared to the sham group). N=4 for each time point (sham, d7, d14, d28). Data are expressed as mean ± SEM.

D. Localization of the Iba1, a microglia marker, in the ipsilateral dorsal horn at d7, d14, and d28 after sciatic nerve cuffing compared to the sham group.

The bar graph shows the percentage of Iba1 positive area. Data are expressed as mean ± SEM. $^{**}p < 0.01$. Dunnett's test (compared to the sham group). N=4 for each time point (sham, d7, d14, d28). Bars: (D1) 200μm; (D2-5) 100μm.

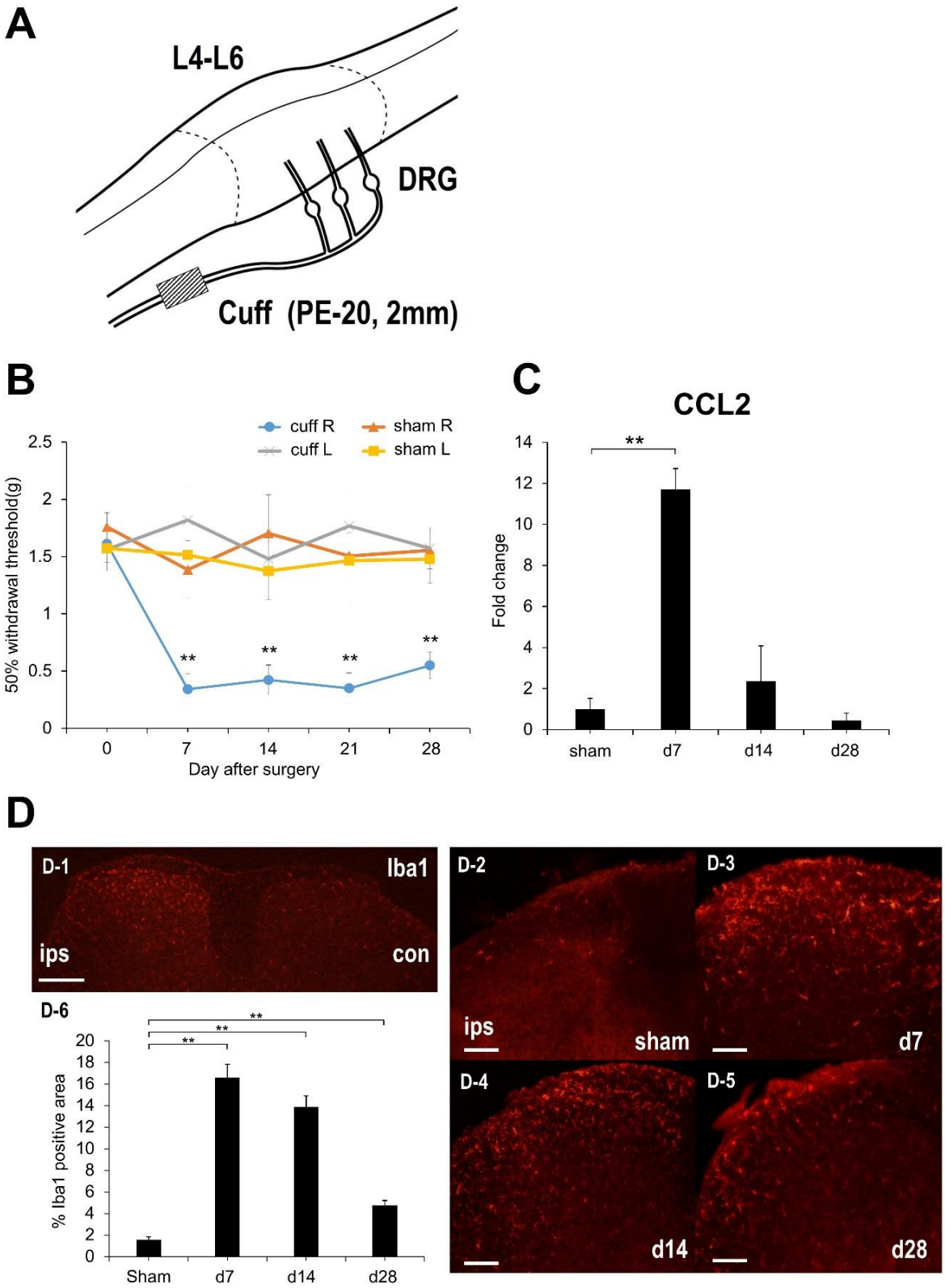
A
L4-L6
DRG
Cuff (PE-20, 2mm)
B
cuff R
cuff L
sham R
sham L
50% withdrawal threshold(g)
Day after surgery
C
CCL2
Fold change
sham
d7
d14
d28
D
D-1
Iba1
ips
con
D-6
% Iba1 positive area
Sham
d7
d14
d28
D-2
ips
sham
D-3
d7
D-4
d14
D-5
d28

Figure 2. Expression profiles of DEGs in the L4-5 spinal cord after sciatic nerve cuffing.

A. MA plot of DEGs in the cuff group compared with the sham mice.

Red dots represent DEGs and black dots represent non-DEGs, respectively. FDR<0.01. X-axis: mean expression, Y-axis: log fold change.

B. Heat map of DEGs in the d28 group compared with the sham group.

Color scale resembles the level

of gene expression in log10 (FPKM+1). Samples of sham and d28 groups are categorized into different categories, respectively.

C, D. The list of the top 20 up and downregulated genes in the mouse neuropathic pain model in the chronic phase, respectively. m. value: log2-fold change.

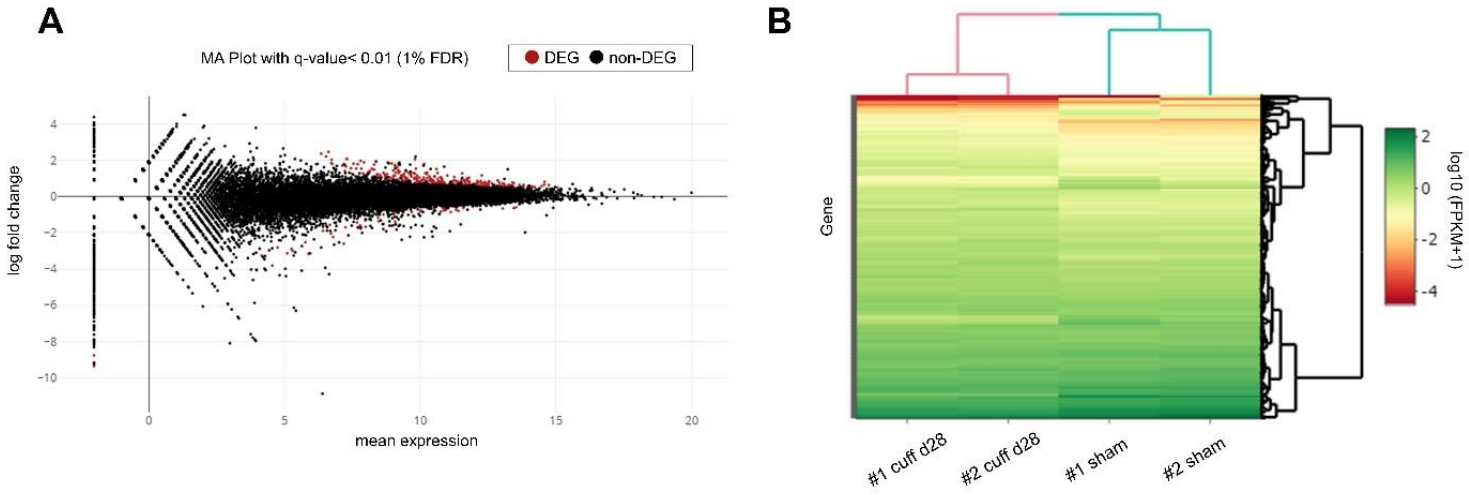

C

Rank	Gene name	m.value
1	sacsin(Sacs)	2.48
2	glutamate receptor, ionotropic, NMDA2A (epsilon 1)(Grin2a)	2.38
3	protein prenyltransferase alpha subunit repeat containing 1(Ptar1)	2.23
4	RAR-related orphan receptor alpha(Rora)	2.10
5	zinc finger protein 369(Zfp369)	2.09
6	homeodomain interacting protein kinase 2(Hipk2)	2.07
7	docking protein 6(Dok6)	2.05
8	erb-b2 receptor tyrosine kinase 4(Erbb4)	1.99
9	cyclin-dependent kinase-like 5(Cdkl5)	1.91
10	family with sequence similarity 135, member B(Fam135b)	1.90
11	potassium voltage-gated channel, subfamily H, member 7(Kcnh7)	1.87
12	argonaute RISC catalytic subunit 3(Ago3)	1.85
13	zinc finger and BTB domain containing 16(Zbtb16)	1.82
14	contactin associated protein-like 5C(Cntnap5c)	1.81
15	protocadherin 11 X-linked(Pcdh11x)	1.81
16	tripartite motif-containing 56(Trim56)	1.80
17	immunoglobulin superfamily, member 9B(Igsf9b)	1.79
18	potassium voltage-gated channel, subfamily Q, member 3(Kcnq3)	1.79
19	LMBR1 domain containing 2(Lmbrd2)	1.75
20	centrosomal protein 85-like(Cep85l)	1.73

D

Rank	Gene name	m.value
1	fatty acid binding protein 1, liver(Fabp1)	-9.35
2	major urinary protein 3(Mup3)	-9.15
3	cytochrome P450, family 2, subfamily j, polypeptide 13(Cyp2j13)	-8.76
4	cytochrome P450, family 2, subfamily j, polypeptide 13(Cyp2j13)	-6.11
5	predicted gene 2260(Gm2260)	-6.00
6	transmembrane protein 233(Tmem233)	-5.90
7	ATPase, H+ transporting, lysosomal V0 subunit D2(Atp6v0d2)	-5.73
8	matrix metallopeptidase 13(Mmp13)	-4.02
9	arginase, liver(Arg1)	-3.80
10	carbonic anhydrase 1(Car1)	-3.24
11	acid phosphatase 5, tartrate resistant(Acp5)	-3.14
12	solute carrier family 38, member 4(Slc38a4)	-3.12
13	pro-platelet basic protein(Ppbp)	-2.98
14	plasminogen(Plg)	-2.88
15	predicted gene 5415(Gm5415)	-2.79
16	myeloperoxidase(Mpo)	-2.58
17	immunoglobulin-like and fibronectin type III domain containing 1(Ifgn1)	-2.50
18	proteoglycan 2, bone marrow(Prg2)	-2.21
19	aquaporin 1(Aqp1)	-2.02
20	lymphocyte antigen 6 complex, locus C2(Ly6c2)	-1.87

Figure 3. Comparison of gene expression profiling between acute and chronic pain phase.

A, B. The top 20 significantly enriched GO/KEGG terms.

A. Analysis of the gene profile in the acute pain phase. The most enriched terms were related to immune response and inflammation. B. Analysis of gene profile in chronic pain phase. The most enriched terms were related to the regulation of cell projection and dendrite.

C. Heatmap of enriched terms comparing acute with chronic pain phase.

We selected the term with the best p-value within each cluster as its representative term and displayed them in a dendrogram. The p-values color the heatmap cells. White cells indicate the lack of enrichment for that term in the corresponding gene list.

D. The Circos plot.

The Circos plot shows how genes from the input gene lists overlap. On the outside, each arc represents the identity of each gene list. On the inside, each arc represents a gene list, where each gene has a spot on the arc. Dark orange color represents the genes that appear in multiple lists, and light orange color represents genes unique to that gene list. Purple lines link the same gene that was shared by multiple gene lists. Blue lines link the different genes where they fall into the same ontology term.

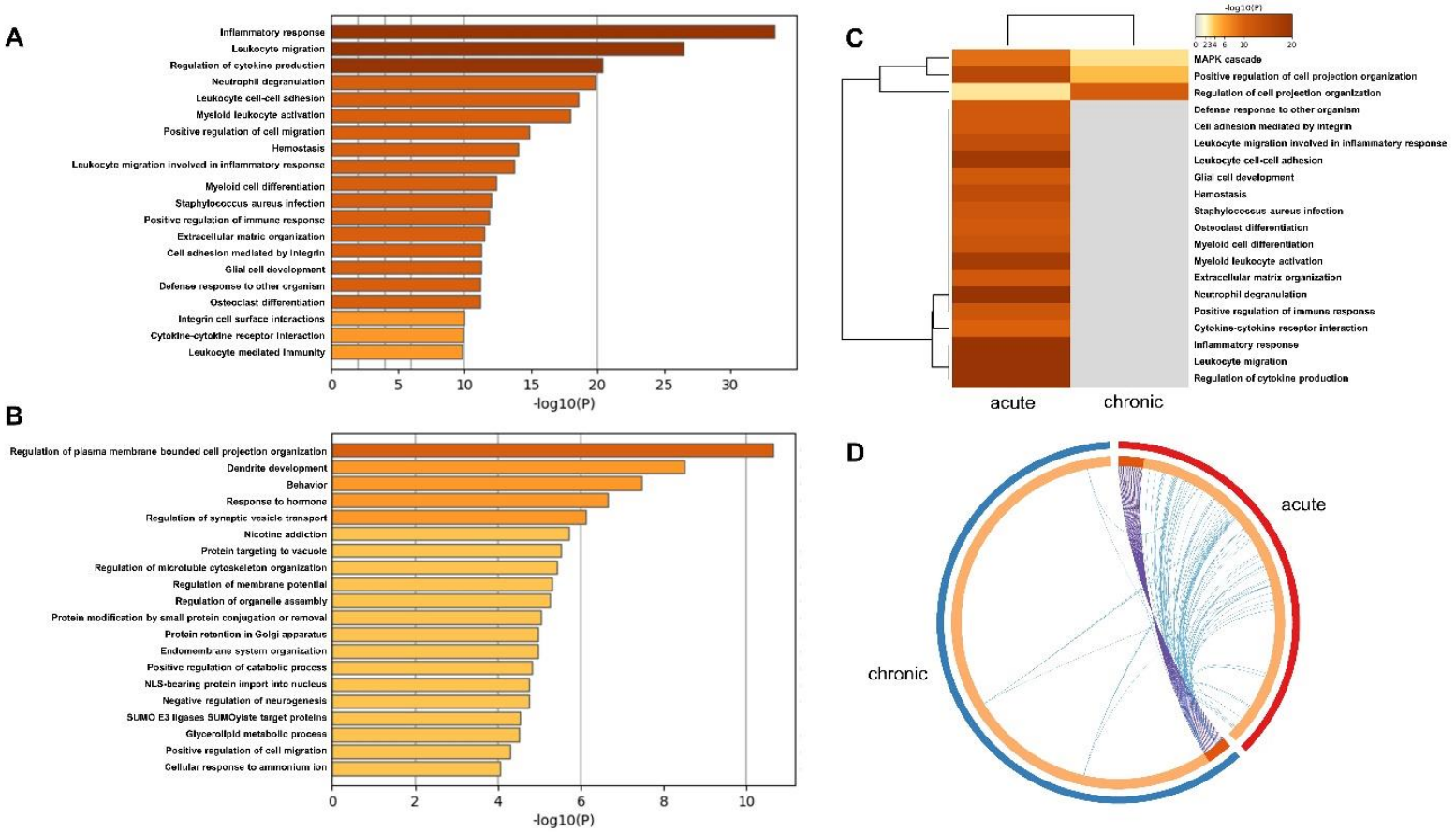

Figure 4. CDKL5 expression in the spinal cord

A. Real-time PCR validation assay for CDKL5 expression in the ipsilateral dorsal horn.

We harvested the ipsilateral dorsal horn of the cuff model and compared the expression of CDKL5 mRNA between the cuff and sham groups. * $p<0.05$. Student's t-test. N=4 for each time point. Data are expressed as mean ± SEM.

B. Localization of CDKL5-expressing cells in the dorsal horn.

B1-4. Co-staining of CDKL5 (green) and proliferation marker CGRP and VGLUT1. CDKL5 was broadly expressed, and Co-staining with CGRP (main projections in lamina I, IIo,) and VGLUT1(a marker of myelinated A fiber that mainly projects to lamina III) did not detect a distinct expression difference of CDKL5 between layers. B5-7. CDKL5 positive cells (green) overlapped with NeuN, a marker of a neuron, staining (red). B8-10. Co-staining of CDKL5 (green) and DAPI. CDKL5 staining showed partial overlap with DAPI and subcellular localization in the cytoplasm. Bars: (C1-4) 100μm; (C5-7) 20μm; (C8-10) 10μm.

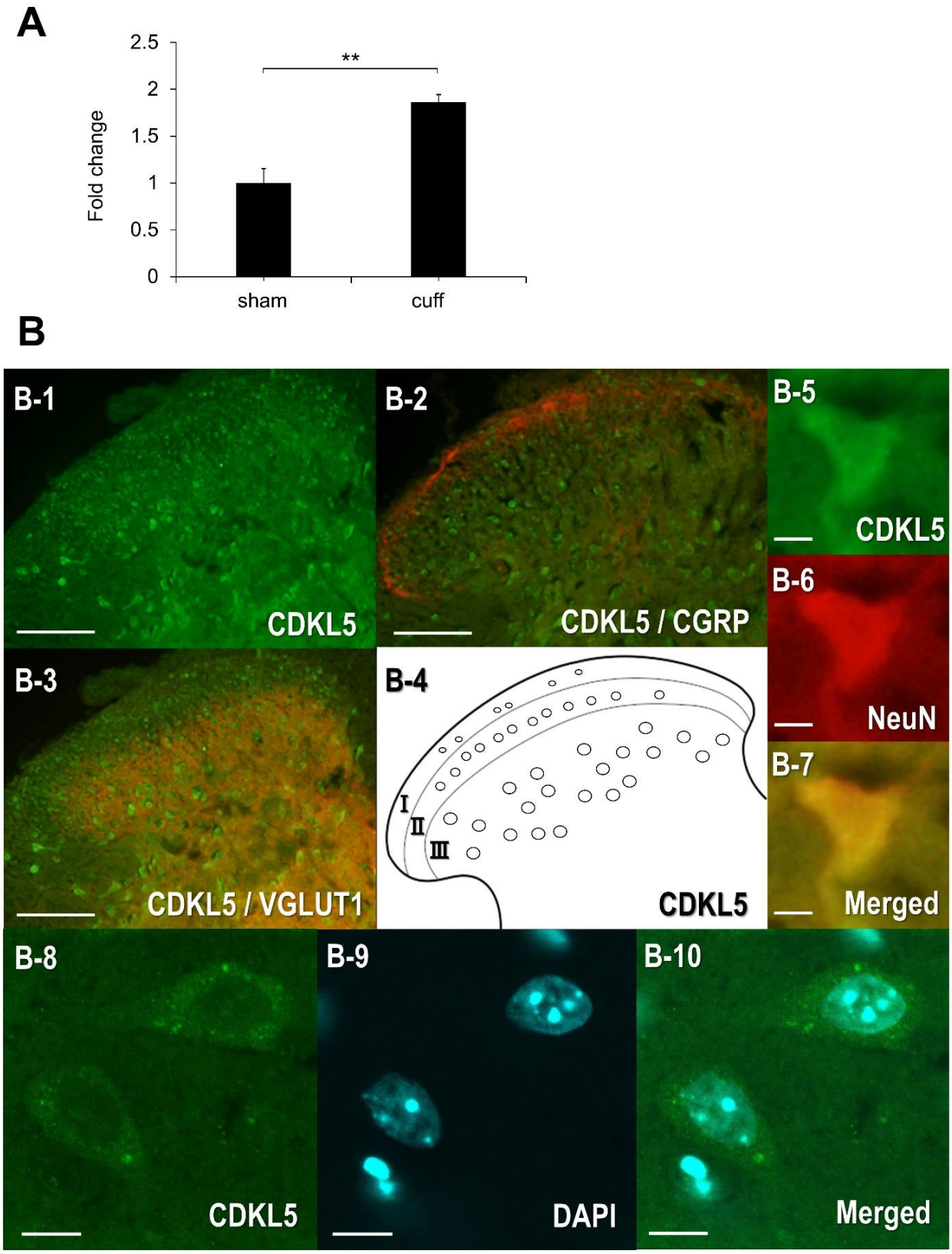
A
2.5
2
1.5
1
0.5
0
Fold change
**
sham
cuff
B
B-1
CDKL5
B-2
CDKL5 / CGRP
B-5
CDKL5
B-6
NeuN
B-3
CDKL5 / VGLUT1
B-4
I
II
III
CDKL5
B-7
Merged
B-8
CDKL5
B-9
DAPI
B-10
Merged

Figure 5. Subcellular localization and effects on neurite outgrowth of CDKL5 mutants

A. Schematic illustration of the DNA constructs.

Three DNA constructs (WT human CDKL5, NLS-attached, and K42R kinase-dead mutant) were used in the present study.

B. The subcellular localization of CDKL5 mutant in HEK293 cells.

We transfected each plasmid DNA into HEK293 cells. At 24h after transfection, Immunofluorescence images show the subcellular localization of CDKL5. (WT and K42R kinase-dead mutant were fused with the GFP gene. NLS-attached CDKL5 plasmid was tagged with FLAG, and anti-FLAG antibody staining was performed in Figure B2-4). WT and K42R kinase-dead CDKL5 were distributed in both the nucleus and cytoplasm. NLS-attached CDKL5 was only distributed in the nucleus. Bars: 50μm.

C. The effects of CDKL5-forced expression on neurite outgrowth of N2a cells.

We transfected each plasmid DNA into N2a cells with an empty plasmid encoding GFP at the ratio of 5:1. The immunofluorescence images show the morphology of N2a cells 36h after treatment with differentiating cell media (DMEM+2%FBS). The percentage of "neurite-bearing" cells in the WT group was significantly higher than that in the control group. Data are expressed as mean ± SEM. **p<0.01, Dunnett's test (compared to the control). Bars: 20μm.

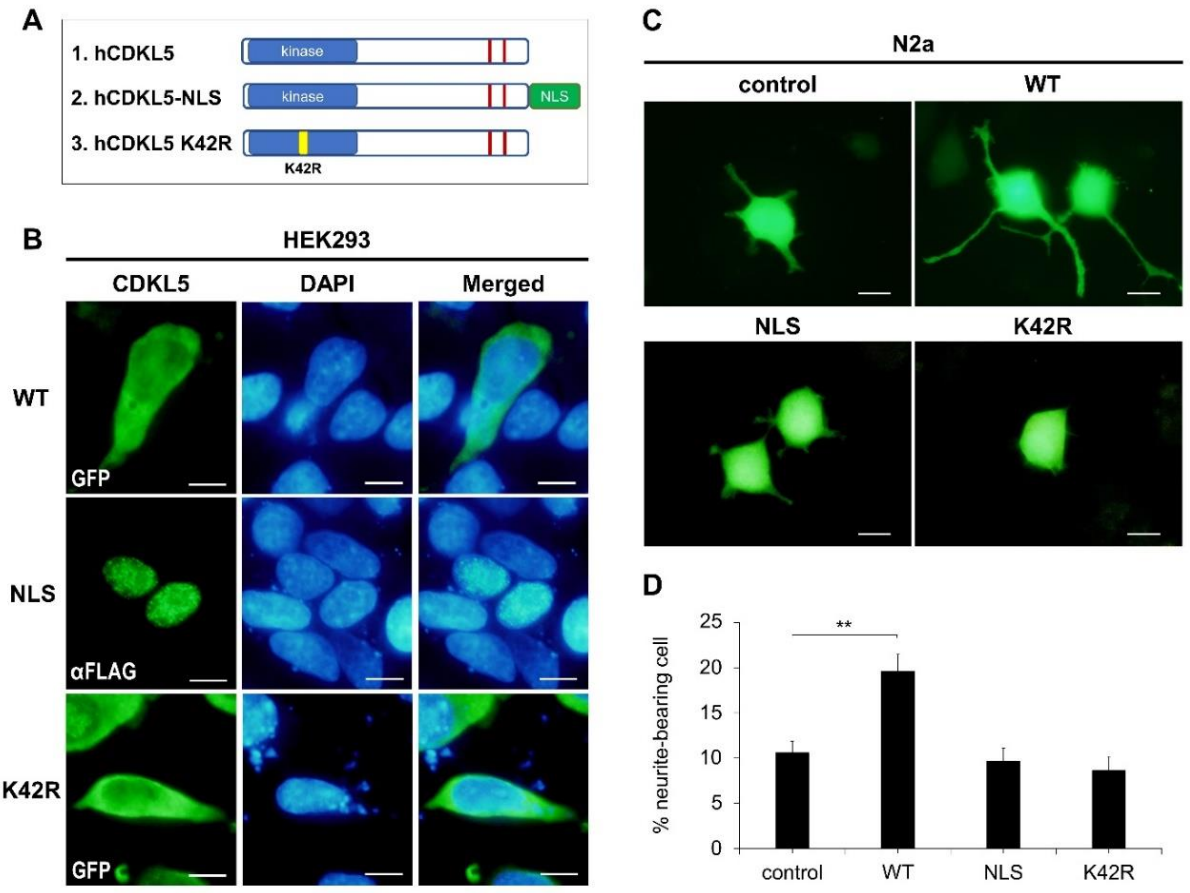

Neuroscience Letters, Volume 749 No 135772

2021 年 2 月 20 日　公表済

DOI: 10.1016/j.neulet.2021.135772